Observations of an atmospheric chemical equator and its implications for the tropical warm pool region

Jacqueline F. Hamilton,[1] Grant Allen,[2] Nicola M. Watson,[1] James D. Lee,[1] Julie E. Saxton,[1] Alastair C. Lewis,[1] Geraint Vaughan,[2] Keith N. Bower,[2] Michael J. Flynn,[2] Jonathan Crosier,[2] Glenn D. Carver,[3] Neil R. P. Harris,[3] Robert J. Parker,[4] John J. Remedios,[4] and Nigel A. D. Richards[5]

Received 8 February 2008; revised 16 June 2008; accepted 29 August 2008; published 31 October 2008.

[1] This paper reports observations of a tropospheric chemical equator in the Western Pacific region during the Austral monsoon season, separating the polluted Northern Hemisphere from the cleaner Southern Hemisphere. Measurements of carbon monoxide, ozone, aerosol size/composition, and non-methane hydrocarbons were made from aircraft, flying north from Darwin, Australia as part of the Aerosol and Chemical Transport In tropical conVEction (ACTIVE) campaign. A chemical equator, defined as a sharp gradient in the chemical background, was found not to be coincident with the Intertropical Convergence Zone during this period. A pronounced interfacial region was identified between 8.5 and 10°S, where tracer mixing ratios increased rapidly within the boundary layer, e.g. CO from 40 ppbv to 160 ppbv within 0.5° latitude (50 km), with inhibited inter-hemispheric mixing. These measurements are discussed in context using a combination of meteorological and Earth-observing satellite imagery, back trajectory analysis and chemical model data with the conclusion that air flowing into and subsequently uplifted by the active convection of the Tropical Warm Pool (TWP) region in the Western Pacific is likely to be highly polluted, and will perturb the composition of the Tropical Tropopause Layer. The main source of CO and other pollutants within the TWP region is expected to be biomass burning, with extensive fires in North Sumatra and Thailand during this period. The sharp gradient in composition at the chemical equator seen here results from extensive burning to the north, contrasting with pristine maritime air advected from the Southern Indian Ocean by a strong land-based cyclone over the Northern Territory of Australia.

Citation: Hamilton, J. F., et al. (2008), Observations of an atmospheric chemical equator and its implications for the tropical warm pool region, *J. Geophys. Res.*, *113*, D20313, doi:10.1029/2008JD009940.

1. Introduction

[2] The shallow coastal waters of the Western Pacific have some of the highest sea surface temperatures in the world and are collectively described as a Tropical Warm Pool (TWP), covering the area roughly between 10° N and 10° S of the equator and from 130° E to 167° E. This warm body of water supplies heat and moisture to the atmosphere above it, causing the formation of deep convective cloud systems that produce high-altitude cirrus clouds. The inter-seasonal variability in the convective and thermodynamic properties of the TWP are discussed by *Reid and Gage* [1996]. These cloud systems affect the amount of solar energy reaching the surface of the Earth as well as the amount of heat energy that can escape into space (e.g. *Jensen and Del Genio*, 2003).

[3] Furthermore, the uplift of boundary-layer air heated by the warm ocean surface to the Tropical Tropopause Layer (TTL) by deep convection in this region impacts on its composition throughout the tropics, and thereby contributes to the chemical species entering the stratosphere in the ascending branch of the Brewer-Dobson circulation. To enable global models to better represent the TTL the composition of the air entering it in deep convection needs to be understood.

[4] During Northern Hemisphere winter (December-March) the Intertropical Convergence Zone (ITCZ), conventionally defined as a low pressure region circling the globe where the trade winds from the Northern and Southern hemispheres meet, typically lies between 10°S and the equator. It is characterized by rapid vertical motion and heavy rainfall, effectively providing a meteorological barrier to cross-equatorial flow in the troposphere with exchange time constants typically around one year [*Bowman*

[1]Department of Chemistry, University of York, Heslington, York, UK.
[2]Centre for Atmospheric Science, University of Manchester, Manchester, UK.
[3]Department of Chemistry, University of Cambridge, Cambridge, UK.
[4]Earth Observation Science, Space Research Centre, Department of Physics and Astronomy, University of Leicester, Leicester, UK.
[5]Institute for Atmospheric Science, School of Earth and Environment, University of Leeds, Leeds, UK.

0148-0227/08/2008JD009940$09.00

and Cohen, 1997] and is well-defined dynamically up to altitudes of 3 or 4 km, above which it is less distinct. It effectively divides the more pristine atmosphere of the Southern Hemisphere from the polluted Northern Hemisphere. Uplifted air is detrained and returns either north or south to its respective hemisphere of origin in line with the classic Hadley Circulation model, although cross-equatorial mixing at altitudes above 5 km has been observed [*Gregory et al.*, 1999].

[5] During the period studied (January-February), the meteorology of Northern Australia is dominated by the Australian-Indonesian monsoon. The monsoon refers to a seasonal reversal of surface-level wind direction. In Northern Australia, the dominant flow in the dry season is south-easterly, whereas the flow during the monsoon is north westerly. The wet season is characterized by episodes of monsoon flow lasting 1–2 weeks, punctuated by break conditions when the monsoon trough lies to the north, and the lower tropospheric flow is generally easterly [*May et al.*, 2008]. The monsoon trough is a zone of convergence characterized by low surface pressure and widespread deep convection. During the monsoon season the low pressure monsoon trough and the ITCZ can be regarded as the same phenomena.

[6] Carbon monoxide (CO) is an ideal tracer to study the transport of pollution with an atmospheric lifetime of 1 to 2 months typical of hemispheric transport timescales. It also has relatively simple chemistry and removes a large fraction of OH radicals in the troposphere [*Thompson*, 1992]. The main atmospheric sources of CO are *via* the photo-chemical degradation of methane and other volatile organic compounds and direct emissions from the incomplete combustion of fuels (predominately biofuels and biomass burning in this region). Previous studies of atmospheric pollutants on either side of the ITCZ indicate a gradient in CO and other pollutants between hemispheres, the magnitude of which is highly dependent on location. For example, the Pacific Exploratory Mission-Tropics B (PEM-Tropics B) took place in the remote Pacific Ocean where pollution sources are minimal and elevated pollutants are likely the result of long-range transport. Within the boundary layer, the average mixing ratios of CO were reported to be around 6–15 ppbv higher north of the ITCZ than on the southern side [*Gregory et al.*, 1999]. In contrast, the Indian Ocean Experiment (INDOEX), [*Mitra*, 2004] was conducted in the Indian Ocean, where the area to the north of the ITCZ is South East Asia and India, home to nearly a third of the world population; and to the south lies the Southern Ocean, one of the most pristine environments on the planet. Aircraft measurements during INDOEX indicated that the large difference in pollutant sources and strengths produced a much steeper gradient either side of the ITCZ with average CO mixing ratios of 175 ppbv and 49 ppbv at 5°N and 5°S respectively [*Williams et al.*, 2002]. This was confirmed by ship measurements, where CO and ozone increased by a factor of three and four respectively as the ship crossed the ITCZ region. The transition between hemispheres observed on the boat was sharp over the course of a single day, indicating that the ITCZ is an effective barrier to mixing [*Stehr et al.*, 2002].

[7] Although aircraft measurements allow direct observation of such chemical differences, active convection associated with the ITCZ makes it difficult to investigate this boundary region, whilst ship measurements are restricted to the lowest level of the atmosphere and require long mission times to sample large areas. The majority of previous atmospheric studies in the tropics have identified the ITCZ as the main boundary to inter-hemispheric mixing. In this study we provide evidence for a sharply defined and narrow atmospheric boundary between hemispheres which did not coincide with the ITCZ or monsoon trough during the measurement period.

[8] These measurements were made during two specialized aircraft missions as part of the ACTIVE campaign on 30 January and 3 February 2006 (for further details of the ACTIVE campaign, see [*May et al.*, 2008; *Vaughan et al.*, 2008]). We introduce here the generic term "chemical equator" to describe a defined boundary between air of northern and southern hemispheric origin with inhibited inter-hemispheric mixing. An extensive suite of high time resolution measurements across the boundary of pollution tracers, such as CO, ozone, aerosol properties and non-refractory composition, will be presented and a comparison will be made of the chemical characteristics on each side. Back trajectory analysis is employed to determine air mass origin, indicating that biomass burning sources in South East Asia are an important source of CO in the air to the north of the chemical equator. In situ measurements of CO will be compared to satellite measurements and model simulations and the implication for the tropical warm pool region will be discussed.

2. Instrumentation

2.1. Aircraft

[9] The aircraft measurements presented here were taken using the U.K. Natural Environment Research Council Dornier 228-01 operated by the Airborne Research and Survey Facility (ARSF). This twin turbo-prop, non-pressurized aircraft accommodates two pilots, one mission scientist and two instrument scientists. The maximum altitude of the Dornier is 8230 m and it has a range and endurance of 1270 nautical miles and 7½ hrs at a typical science altitude of 1500 m. Its typical speed on the flights described here was 80 m s^{-1}. The aircraft was used to characterize the boundary layer and lower levels of the free troposphere during ACTIVE and generally operated below 3500 m. The aircraft was fitted with an Aircraft Integrated Meteorological Measurement System (AIMMS-20, Aventech Research Inc.), a wing-mounted probe which provides pressure, temperature, relative humidity, GPS data, wind and velocity. An optimized air inlet (Deutsches Zentrum für Luft- und Raumfahrt, DLR) was mounted on top of the aircraft for aerosol and gas measurements.

2.2. Carbon Monoxide

[10] Measurement of CO was performed in-flight using a fast response fluorescence instrument, AL5002 carbon monoxide (CO) monitor, (Aero-Laser GmbH, Garmisch-Partenkirchen, Germany), fitted with a Nafion dryer to remove water vapor. With an integration time of 10 seconds the detection limit was better than 2.0 ppbv. The linearity range of the instrument was 0–100 ppmv, encompassing the mixing ratios encountered during these flights. Calibration

of the instrument was performed in-flight at each altitude level, to allow for any effect of ambient pressure changes, using a secondary gas standard containing 73 ppbv ± 5% CO in air. A primary standard (200 ppbv in air) was used throughout the campaign to validate the in-flight standard. Data were collected at 1 s intervals.

2.3. Ozone

[11] Ozone was measured in-flight using a UV absorption detector (2B Technologies) fitted with a Nafion dryer to remove water vapor. Calibration was carried out prior to deployment using gas phase titration of NO. Data were collected at 10 second intervals with an overall uncertainty of 5% or ± 2 ppbv, whichever is greater.

2.4. Volatile Organic Compounds

[12] VOCs were collected onto absorbent tubes using an Automated Tube Sampler (ATS) developed at the University of York. Fifteen pre-packed absorbent tubes (Thames Restek) (Carbopack C, Carbopack B and Carbosieve III) were fitted into a block held at 19°C, controlled by Peltier cooling and a wire coil heater. A sample flow of 200 ml min^{-1} for 5 minutes, gave a total sample volume of 1 L. A stainless steel bellows oil-free pump (KNF, UK) was used to pressurize the sample through the ATS with a relief valve fitted to ensure the sample pressure remained constant regardless of altitude. Absorbent tubes were cleaned prior to each flight (90 minutes at 350°C under a helium flow of 30 ml min^{-1}) and immediately after landing were removed from the ATS, sealed with brass nuts and placed in sealed containers until analysis.

[13] Tubes were analyzed post-campaign using gas chromatography (GC) (HP6890, Agilent Technologies) coupled to time-of-flight mass spectrometry (Pegasus III, Leco). Tubes were spiked with 30 ml of d_8-toluene gas standard and transferred to a secondary tube *via* a cold finger at 0°C to remove water. Transferred samples were thermally desorbed using an Automated Thermal Desorption system (Perkin Elmer) coupled to the GC column via a heated transfer line. After purging with helium, analytes were desorbed at 325°C for 5 min onto a secondary cold trap held at −30°C, which was then rapidly heated to 350°C at 40°C min^{-1}. Separation was achieved using a 60 m × 0.25 mm × 1 μm 5%-phenyl-methylpolysiloxane BP5 column held at a constant pressure of 23 psi helium. Calibration was achieved using a 74 component gas standard at 0.1–2 ppbv levels (Apel Riemer).

2.5. Aerosol Measurements

[14] Aerosol particle number size distributions from 55 nm to 32 μm diameter were measured using a range of optical probes (see *Allen et al.* [2008] for further details). A Grimm optical particle counter and a Droplet Measurement Technologies (DMT) Aerosol Spectrometer Probe (ASP) measured overlapping size ranges from 0.3 to 25 μm, and 0.21 to 4.5 μm, respectively, with corresponding size resolutions of 0.1 to 0.2 μm and 0.03 to 0.5 μm. However, inlet transmission considerations (50% transmission at 2.5 μm) limit quantitative measurements by these probes to a 2 μm upper limit. For the larger aerosol component, an open-path, wing-mounted Forward Scattering Spectrometer Probe (FSSP), described by *Baumgardner et al.* [1985], was used to measure particle number size distributions from 1.5 to 32 μm, sampling air directly in the incident air stream. In addition, a TSI 3010D condensation particle counter (CPC) measured the total particle number concentration greater than 10 nm (up to the inlet cut-off diameter) by condensational growth in a supersaturated butanol chamber [*Agarwal and Sem*, 1980] and a Radiance Research Particle Soot Absorption Photometer (PSAP) measured aerosol black carbon content by measurement of the progressive decrease in optical transmission of a filter caused by particle deposition using an integrated plate technique.

[15] For aerosol composition measurements, a Quadrupole Aerosol Mass Spectrometer (Q-AMS) system [*Jayne et al.*, 2000] which sampled air through the main inlet manifold, was used to determine the chemical composition of the non-refractory, non-sea-salt component of sub-micron aerosol using a data analysis procedure described by *Jimenez et al.* [2003] and *Allan et al.* [2003]. For ACTIVE, the Q-AMS was configured to sample aerosol between 40 and 700 nm with 100% transmission, decreasing to 50% transmission at 1 μm. Mass concentrations are reported for the overall nitrate, organic, sulphate and ammonium aerosol components.

3. Meteorology

[16] Towards the end of January 2006, a monsoon low pressure system moved south and inland from Darwin, settling over the middle of the Northern Territory, leading to an inactive monsoon in the Darwin area [*May et al.*, 2008]. This was characterized by strong westerly winds (30 to 40 knots) and isolated showers confined below around 10 km, contrasting markedly with an earlier more convectively active monsoon phase in early January, which was characterized by widespread organized deep convection. On the day of the first flight on 30 January, the Western Pacific region was dominated by a large band of convection (running south west from 120°E, 10°N to 180°E, 30°S and over 100 km wide). The monsoon low had intensified over the previous few days forming a highly active convective region between Darwin and Alice Springs (see Figure 1). During the same period, a tropical cyclone (TC Jim) also developed in the Coral Sea and moved in a south easterly direction. The monsoon depression reached a minimum pressure of 989 hPa on 31 January then began to weaken over the next 48 hrs. By the second flight on 3 February, the region north of Darwin was influenced by monsoonal squalls and the monsoon low had completely dissipated over the Northern Territory. During this period the ITCZ, using the conventional pressure definition (narrow band of low pressure due to convergence and uplift), lay along the monsoon trough south of Darwin which can clearly be seen in the lower section of Figure 1, and the typical narrow band of cloud seen in satellite-derived descriptions of the ITCZ was not present [*Waliser and Gautier*, 1993].

[17] Figure 1 (upper) shows the infrared satellite imagery of Northern Australia and the Western Pacific region, taken from MTSAT-1R during the research flights designated SD19 on 30 January and SD22 on 3 February. The aircraft instrumentation was not designed to operate in clouds, so active convective regions were avoided. Presented in the

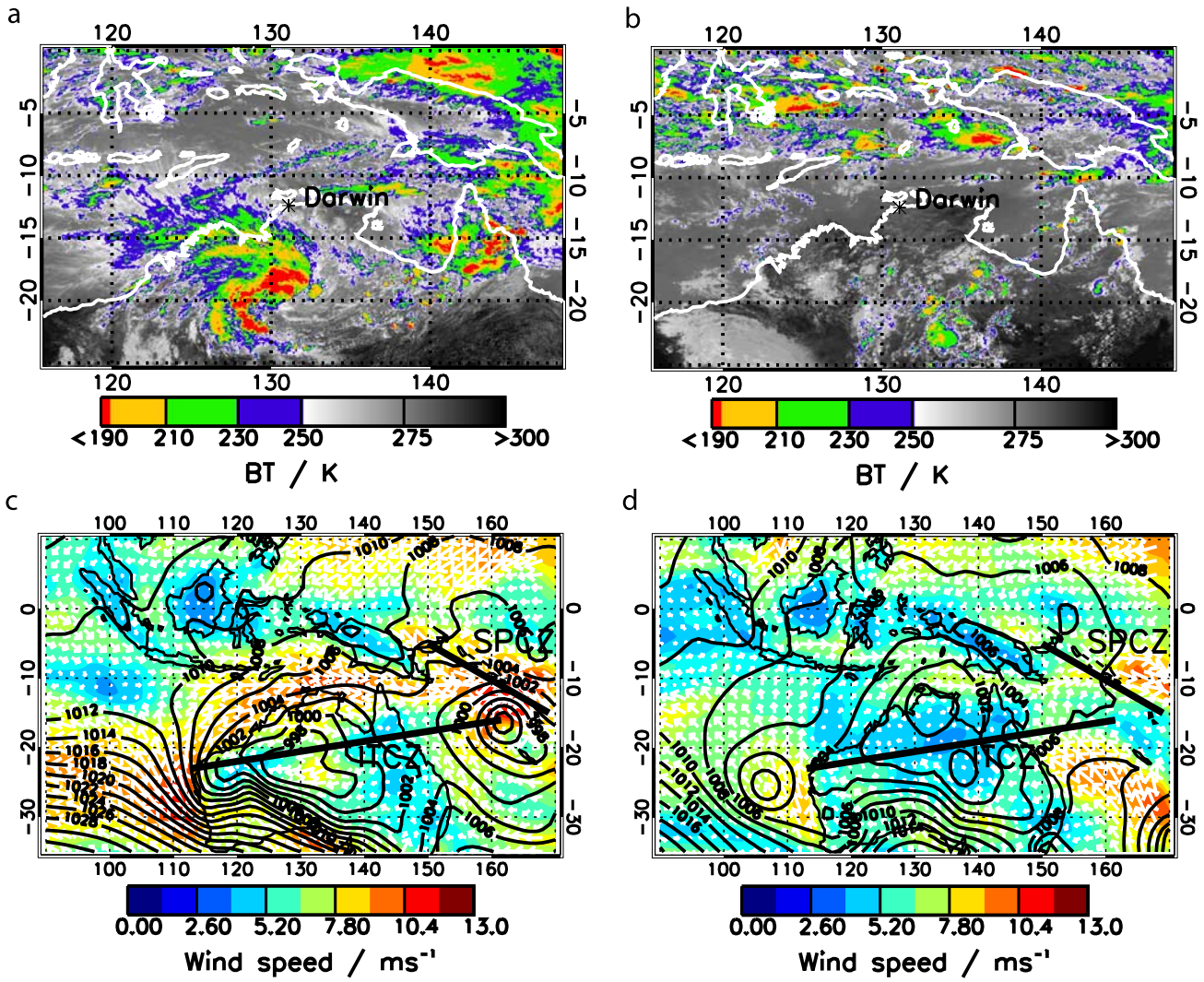

Figure 1. Meteorological data for 30 January 2006, SD19 (left) and 3 February 2006, SD22 (right). Upper: 05:33 hrs UTC (14:03 Darwin local time) MTSAT Infrared images for the Northern Australian region (Areas with T > 250 K are gray scale, 250–230 K are blue shades, 230–210 K are green shades, 210–190 K are yellow shades and T < 190 are red shades, wavelength 10.8 μm). Lower: ECMWF Mean Sea level pressure and 10 m winds, 06:00 hrs UTC on day of flight (15:30 Darwin local time). The positions of the ITCZ and South Pacific Convergence Zone (SPCZ) are denoted by the black lines.

lower section of Figure 1 are corresponding 10 m wind and mean sea level pressure fields taken from the European Centre for Medium Range Weather Forecasts (ECMWF) operational product. The strength of the winds is indicated by both the colored contours and the size of the wind vectors. Clearly seen on 30 January is the strong (>13 ms^{-1}) westerly flow in the Arafura Sea (the maritime region to the north and west, between the Darwin coast and Indonesia) and the confluence of air from north and south upwind of this region. By 3 February the winds have abated and the region of confluence has moved north over the Indonesian island chain. 5 and 10-day back trajectories were calculated using NOAA's Air Research Laboratories Hybrid Single Particle Langrangian Integrated Trajectories (HYSPLIT) program [*Draxler and Rolph*, 2003]. GDAS (NCEP Global Data Assimilation System) met fields were used, which are 3 hourly, 1 × 1 degree fields with 23 vertical levels from the surface to 20 hPa (giving ~50 hPa spacing). For the vertical motion the model vertical velocity was used. It should be noted that the model is not suited to simulate the rapid uplift of air in deep localized convection and thus is used here to look at larger scale transport processes.

4. Flight Tracks

[18] Two flights were carried out to investigate the position and chemical variability across the chemical equator. The first flight designated SD19, took place on 30 January 2006. After take-off at 14:39 local time (all further times will be quoted as Darwin local time) from Darwin Airport (12.41°S, 130.86°E), the aircraft ascended to 1830 m, proceeding SW to approximately 13.0°S, 130°E.

There, it turned to a north-easterly heading, first executing a series of profiles between 1830 and 400 m (with small course corrections to avoid convective towers) then flying at 400 m above the Arafura Sea from 10.9°S, 131.0°E to 9.84°S, 131.99°E. At this point it climbed to 3000 m to reach its furthest point of 8.95°S, 132.38°E. On the homeward leg the aircraft followed a SW course at 3000 m to 9.84°S, 131.97°E before descending to 1030 m, then continued to 10.62°S, 131.63°E where it descended to 730 m for the return to Darwin by 18:46.

[19] The second flight, SD22, took place four days later on 3 February 2006. After take off at 14:10, the aircraft headed along a 30° bearing and climbed to 2300 m, where it carried out a constant pressure altitude run from 12.04°S, 131.00°E to 11.36°S, 131.24°E. It then descended to 730 m, continuing at this level to 8.80° S, 132.39°E. A series of constant pressure altitude runs followed between approximately 8.9° S and 9.7° S at 1330 m, 3134 m and 415 m, before continuing south-westwards at this final height to 11.08°S, 131.46°E. The aircraft then transited back to Darwin at 700 m, landing at 18:30. Altitude time series are shown in Figure 2 and the flight tracks superimposed onto a map of the local area are shown in Figure 3.

5. Results

[20] The time series of CO, O_3, and aerosol size fractions and composition, obtained during flights SD19 and SD22 are shown in Figure 2. Note that aerosol composition measurements from the AMS in Figure 2 are plotted as a 10-point running mean to reduce the noise in the data set. Around Darwin, the air sampled within the boundary layer and the free troposphere was very clean with low levels of CO and aerosols. Mean mixing ratios of CO were 50 ppbv and showed a small increase with increasing altitude (400 m to 2500 m) of around 10 ppbv. As the aircraft flew NE within the marine boundary layer, a sharp increase in pollutant concentrations was observed. CO concentrations rapidly increased from 45 to 160 ppbv over 20 minutes, equivalent to a boundary region around 50 km wide. In order to visualize the position of the chemical equator, the flights tracks in Figure 3 have been color coded for CO concentrations ranging from 40 (purple) to 150 ppbv (red). For SD19 the boundary region between polluted and clean air can clearly be seen and is well defined at around 10.75°S at an altitude of 400 m. At higher levels a more complex picture emerges, with apparent interleaving of CO-poor and CO-rich air, indicative of stirring or differential advection at these altitudes. Four days later, on SD22, the chemical equator had moved further north to 9°S at 400 m. Overlapping flight runs in SD22 make it difficult to see the boundary in Figure 3 (lower), but the representation of latitude versus altitude in Figure 3 (upper), shows the interfacial region clearly. On this flight the boundary was vertically coherent, with far less variation with height than SD19.

[21] Within the boundary layer, elevated CO levels were accompanied by a corresponding increase in atmospheric particles. On SD19, ASP measurements showed a dramatic increase in accumulation mode aerosol (0.2–2 μm), with concentrations increasing from southern hemispheric background levels of 7 particles cm^{-3} to over 100 particles cm^{-3}, while fine and ultra-fine size ranges of particles (0.01–2 μm) measured by the CPC increased from around 300 to 1400 cm^{-3}. Absolute concentrations of both aerosol particles and CO within the polluted air mass were similar on both flight days. Composition measurements using the aerosol mass spectrometer indicate the non-refractory component of the aerosol was dominated by sulphate on SD19 and by sulphate and organics on SD22 but concentrations were significantly lower in the latter flight. Sulphate and nitrate aerosol were on average neutralized by the presence of ammonium (not shown). In the free troposphere, CO correlated well with the smallest particles (the ultra-fine mode measured by the CPC) but there was a significant drop in the concentrations of larger particles compared to the boundary layer, as measured by the ASP, GRIMM and FSSP. Ozone levels were also elevated north of the chemical equator with a maximum concentration of 49 ppbv, in contrast with an average southern hemisphere background level of 20 ppbv. However, the factors controlling the O_3 concentration appear to be more complex than the other pollutants resulting in deviations from the general patterns.

[22] Low time resolution VOC samples were collected north of the chemical equator only during the flights SD19 and SD22. In the period between the flights presented here, the aircraft flew a survey mission to Alice Springs approximately 1500 km to the south of Darwin, to obtain a background southern hemisphere profile of trace gases. This inland region is very sparsely populated and emission sources are minimal. Trajectory analysis indicates that the air sampled in this region had a similar source to the air south of the chemical equator. It is therefore assumed that the VOC data from the survey missions to Alice Springs is indicative of the southern hemisphere air masses sampled on 30 January and 3 February. The median concentrations north and south of the chemical equator for each flight of CO, O_3, and aerosols are given in Table 1 (note that all aerosol data has been filtered to remove incidences of passage through cloud). VOCs are shown as an average for each air mass classification due to limited sample numbers.

6. Discussion

[23] The position of the chemical equator observed by CO tracer concentrations during the flights has been marked on the flight track profiles (Figure 3). It is clear from the satellite imagery (Figure 1) that the chemical equator is not associated with a convectively active region but is in clear sky conditions. Over the preceding days before the flights, the monsoon trough moved southwards over the Northern Territories and increased in intensity forming a highly active convective region between Darwin and Alice Springs. This low pressure system was essentially a land-based cyclone which resulted in strong westerly winds with dry air at mid-levels effectively blocking monsoon convection to the north. Trajectory analysis, for 5 days (see Figure 4 left) and extended further to 10 days (Figure 4 right) indicates that this air stream originated in southern mid-latitudes, flowing northwards then eastwards around the low pressure to isolate the monsoon trough from the Tropical Warm Pool over Indonesia. The crucial feature here is the limited longitudinal extent of the monsoon trough over Australia (Figure 1) and the consequent cyclonic flow around its

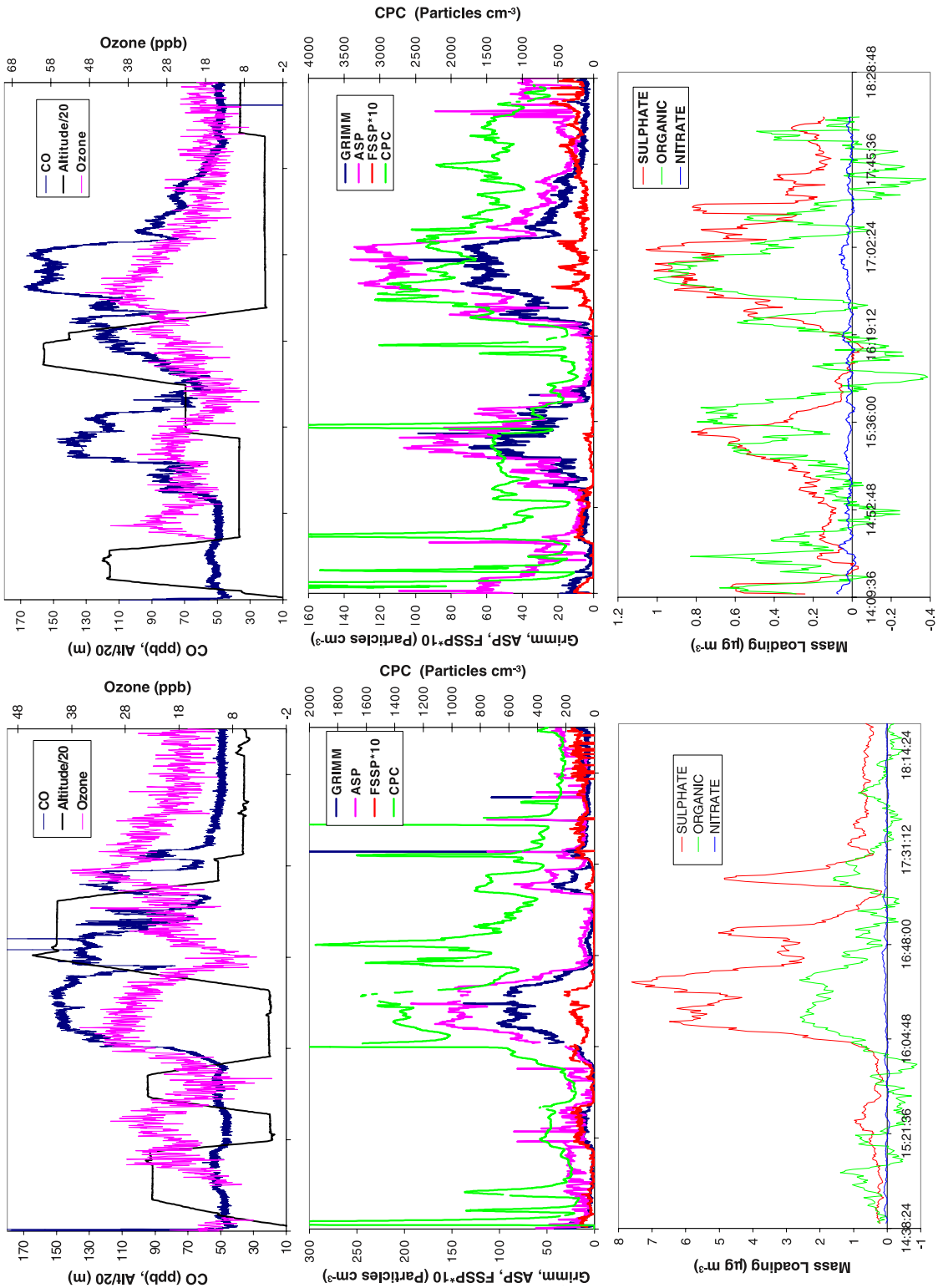

Figure 2. Trace gas and aerosol time series obtained during SD19 (left) and SD22 (right). Upper: CO, O_3 and altitude/20 profiles. Middle: Grimm Particle Counter, Aerosol Spectrometer Probe (ASP), Forward Scattering Spectrometer Probe (FSSP)/10 and Condensation Particle Counter (CPC) concentrations. Lower: Aerosol Mass Spectrometer (AMS) non-refractory, non-sea salt aerosol composition.

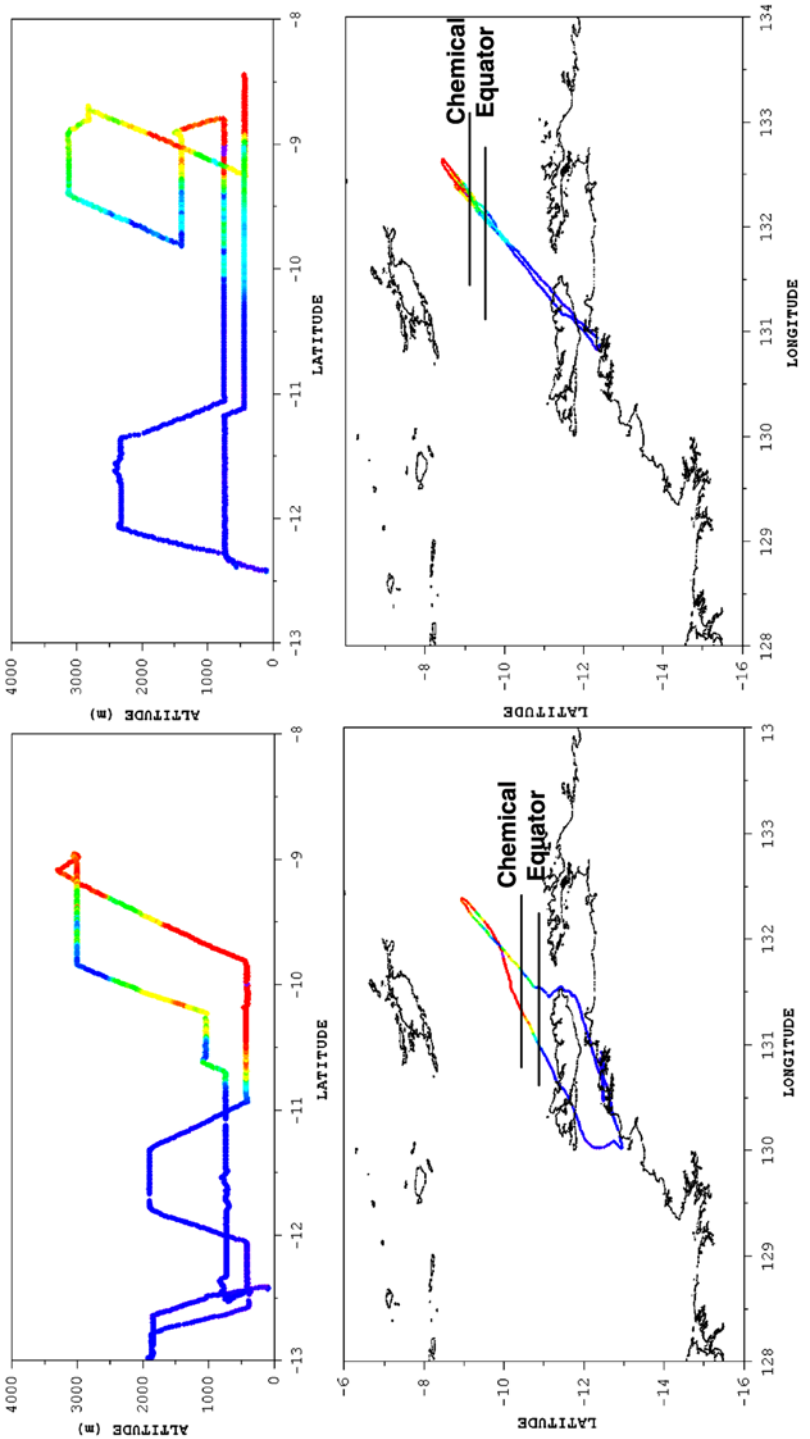

Figure 3. Flight track and altitude profiles colored by CO mixing ratios, from 40 ppbv (purple) to 150 ppbv (red). The position of the chemical equator is indicated by black lines around 10.75°S and 9°S on SD19 and SD22 respectively.

Table 1. Median Mixing Ratios and Concentrations of Trace Gases and Aerosols, Respectively, to the North and South of the Chemical Equator Calculated Across Flights SD019 and SD022[a]

Species Measured	Median Southern Hemisphere Concentration (SD019, SD022)	Median Northern Hemisphere Concentration (SD019, SD022)
Ozone (ppb)	(18, 18)	(23, 26)
Carbon Monoxide (ppb)	(50, 50)	(126, 112)
Aerosols (particles cm^{-3})		
CPC (>10 nm)	(309, 1242)	(705, 1616)
ASP (0.22–2 μm)	(15, 18)	(38, 41)
GRIMM (0.3–2 μm)	(7, 7)	(8, 25)
FSSP (0.5–32 μm)	(0.8, 0.5)	(0.3, 0.5)
Volatile Organic Compounds (ppt)		
Ethylbenzene	5	60
m + p xylene	16	74
o-xylene	5	48
n-propyl benzene	2	30
l-propyl benzene	1	11
3-ethyltoluene	2	9
4-ethyl toluene	2	17
1,3,5-trimethyl benzene	3	28
1,2,4-trimethyl benzene	6	38
1,2,3-trimethyl benzene	2	20
nonane	18	75

[a]Southern hemisphere values are representative of VOC concentrations taken on flights to Alice Springs and the Tiwi Islands between SD019 and SD022.

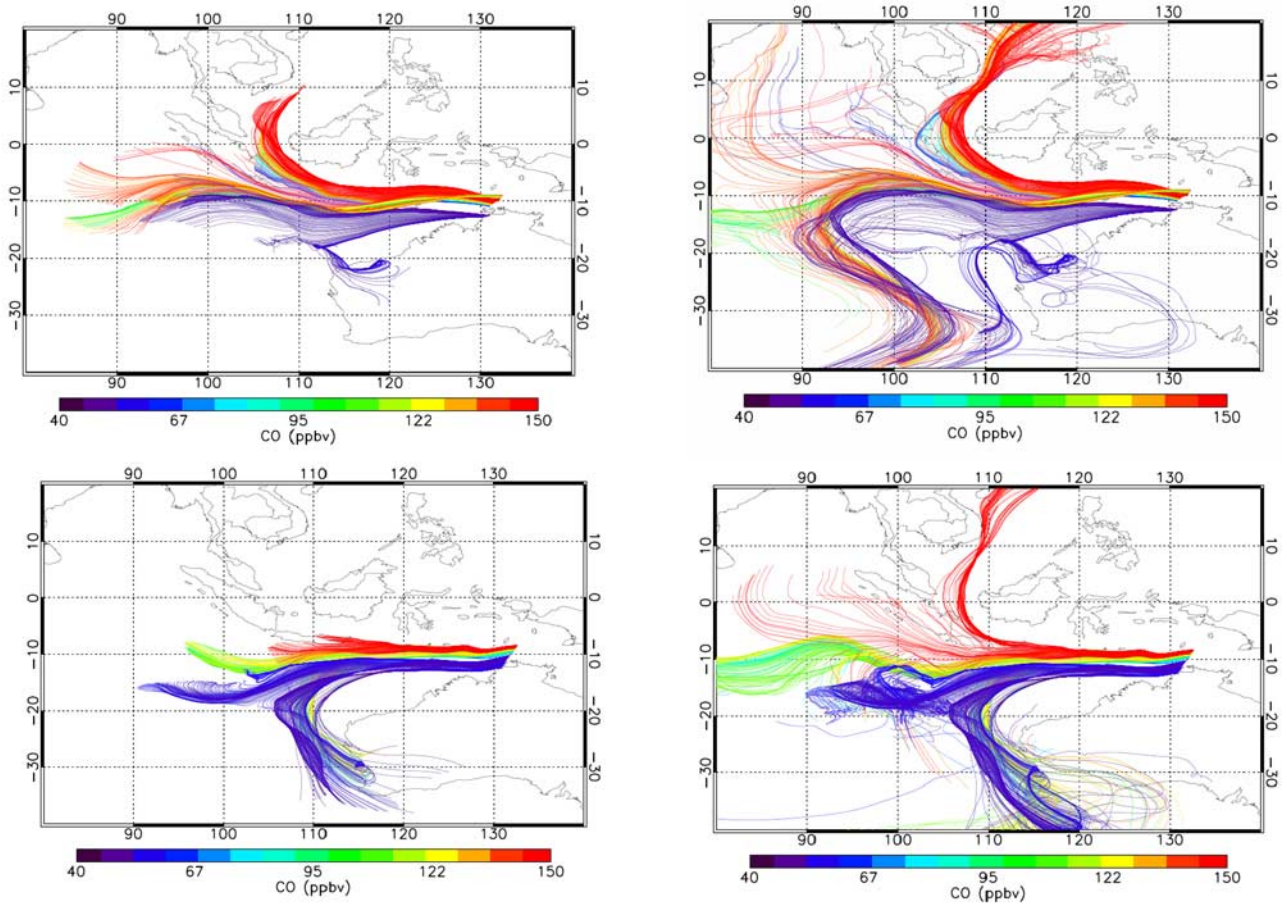

Figure 4. Back trajectories calculated using NOAA's Hysplit model along the aircraft flight track show the switch from air originating in the southern to the northern hemisphere. Upper: SD19. Lower: SD22. Left: 5-day back trajectories. Right: 10 day back trajectories. Trajectories are colored by CO concentrations at trajectory start point on flight track.

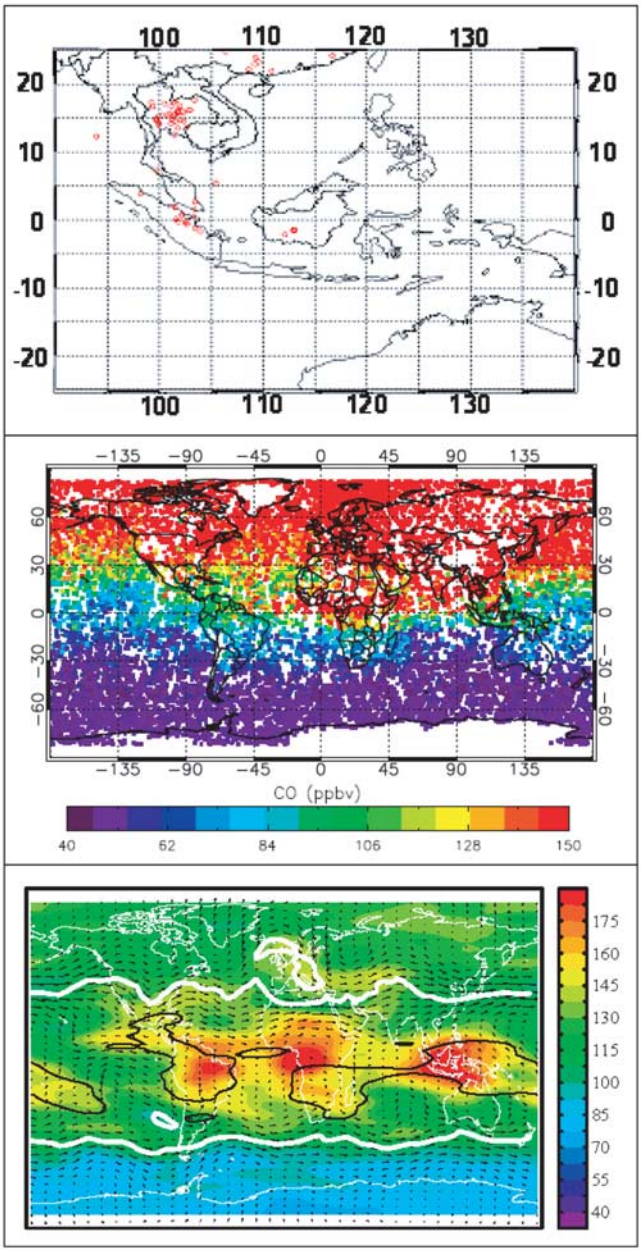

Figure 5. Upper: AASTR fire maps (26 January–31 January 2006). Middle: TES CO profile (ppbv) at approximately 600 mbar (25 January–5 February 2006). Pixels have been enlarged to aid visualization. Lower: Weekly mean upper troposphere MLS Cloud Filtered CO profile (ppbv) at approximately 215 mbar (29 January–4 February 2006). Black lines indicate deep convection (Ice Water Content = 3 mg m^{-3}) and white lines indicate the dynamical tropopause (GMAO Potential Vorticity = 3.5 × 10^{-6} Km^2kgs^{-1}).

western boundary. The chemical equator was therefore caused by confluence between the north-westerly monsoonal flow out of Indonesia and the south-westerly southern hemisphere air flowing cyclonically around the monsoon trough to the south. This resulted in a chemical boundary further north than the ITCZ, away from the regions of convergence and therefore not associated with deep convection.

[24] To determine that the air north of the chemical equator is truly of NH origin, and not highly polluted SH air by some unidentified mechanism, 5 and 10 day back trajectories were initiated from aircraft measurement locations (geographical position and aircraft altitude) shown in Figure 4. Trajectory colors represent the CO concentration observed by the aircraft at the starting point of each trajectory, using the same color range as Figure 3; 40 ppbv (purple) to 150 ppbv (red). The trajectories show a switch in air mass origin within the same region as the chemical equator. On both flight days, air south of the chemical equator was of southerly or westerly marine origin. On 3 February, the influence of the monsoon low over the previous days can clearly be seen, transporting pristine air over Australia's western seaboard from the Southern Indian Ocean, which is unlikely to have been influenced by localized emissions. The low CO trajectories to the south of the CE indicates that the air was well above the boundary layer when traveling over the Australian mainland and descended over the previous two days while traveling over the ocean. Thus they were unlikely to be influenced by emissions from highly populated regions of Australia. 10-day trajectories indicate a Southern mid-latitude origin with air originating in the Southern Indian Ocean to the south and south-west of Australia. Air sampled north of the chemical equator began as north westerly flow 5 days previously, originating well into the northern hemisphere and passing over a number of South Indonesian islands. For SD19, some trajectories north of the chemical equator have a more westerly origin; these correspond to measurements within the free troposphere, where CO concentrations were lower (i.e. colored green on Figure 4). Although the trajectories north of the chemical equator on SD22 have traveled along the boundary region for the previous 5 days, longer trajectory runs (10 days) suggest a South East Asian origin, although longer trajectories are subject to increasing uncertainty due to the compound influences of model limitation as well as localized convection and turbulent mixing which are not resolved. The highest concentrations of pollutant tracers coincide with trajectories which indicate that the air traveled in the boundary layer for much of the previous five days.

[25] Data obtained from the Advanced Along Track Scanning Radiometer (AATSR) on board ENVISAT were used to investigate night-time fire occurrence during the period of the flights [*Arino et al.*, 2005]. A fire count is defined as a saturation of the 3.7 μm channel of the instrument at brightness temperatures greater than 312 K. A composite of fire counts identified in the Western Pacific region between 26 January and 31 January is shown in Figure 5a, where red circles indicate a thermal anomaly. Extensive forest fires were burning in North Sumatra and South East Asia during the end of January 2006. The flights were divided into NH and SH air based on air mass origin from the trajectory analysis. Within the SH air, there was no obvious correlation between CO and O_3 and concentrations were low indicating a well-processed air mass. However, under polluted NH conditions, a clear correlation existed with an O_3: CO ratio of approximately 0.16, consistent with aged biomass burning plumes from South East Asia [*Kondo et al.*, 2004]. The mixing ratios of a wide range of VOCs

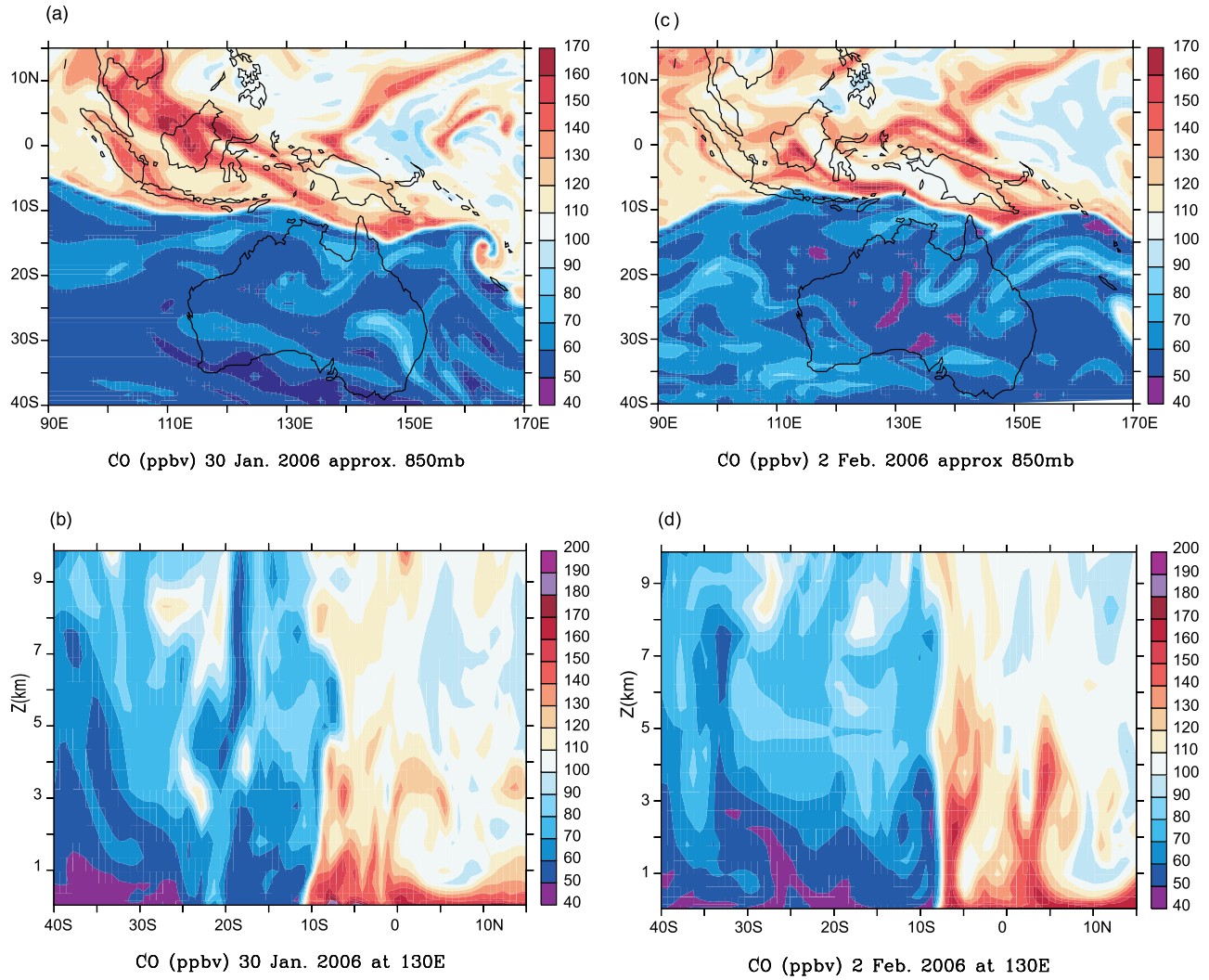

Figure 6. CO modeled using the p-TOMCAT chemical transport model. CO here is advected as a passive tracer having started from a chemically active initial field on 1 January. (a) and (c) show the horizontal section at 12UT at approximately 830mb for 30 January and 3 February respectively. (b) and (d) show the vertical section taken at 130E, close to the flight tracks of SD19 and SD22 for the same days.

shown in Table 1 show a marked contrast between air sampled on each side of the chemical equator. Aromatic hydrocarbons, a marker of fossil fuel combustion, are significantly higher in the Northern Hemispheric air, reflecting enhanced anthropogenic emissions. Thus the elevated levels of pollutants north of the chemical equator are likely the result of a combination of the increased Northern Hemisphere background and biomass burning plumes.

[26] In order to determine the extent of the chemical equator, the global chemical transport model p-TOMCAT, an updated version of the TOMCAT model used for a range of tropospheric modeling studies was used [*Law et al.*, 2000; *O'Connor et al.*, 2004; *Savage et al.*, 2004]. For this case study, p-TOMCAT was run at a horizontal resolution of 0.75 × 0.75 degrees (grid spacing approx. 80 km at the equator) with 31 vertical levels up to 10 hPa. This model is dynamically driven using the European Centre for Medium-Range Weather Forecasts (ECMWF) operational analyses at a horizontal resolution of 3 × 3 degrees. In this study, the model's chemistry, emissions, convective parameterization and boundary layer mixing parameterization were switched off; thus, any features that develop are due to transport by the analyzed winds and not due to any local mixing or chemical processing. The model was initialized from a lower resolution run (that included all the model's processes) on 1 January 2006. Although the modeled CO may not quantitatively compare with observations as emissions are switched off for the high resolution run, the lifetime of CO means modeled CO will qualitatively represent the shape and dynamically induced features of the observed CO. Figure 6 shows horizontal and vertical sections of modeled CO for 30 January and 3 February. The high resolution run shows a striking sharp horizontal gradient in modeled CO close to the observed gradient and simulates well the scale over which the observed CO changes. The model also captures the difference in observed CO concentration both sides of the chemical equator as well as its movement north between 30 January and 3 February as seen in the obser-

vations. The vertical section illustrates the altitude to which the chemical equator is present. A slight northerly tilt of the boundary with altitude on the 30 January and a vertical boundary on 3 February are both consistent with observations. As this model run does not include any convective mixing, the modeled gradients are produced solely by the large scale flow in the analyzed winds.

[27] To assess the implication of the chemical equator's position south of the convectively active TWP region, satellite measurements of CO were used to gain a more regional perspective. The Tropospheric Emission Spectrometer (TES) [*Beer et al.*, 2001] was launched in July 2004 onboard NASA's Aura platform. TES is a Fourier transform infrared spectrometer and was designed to provide simultaneous vertical information on tropospheric ozone, CO and other trace gases on a global basis. The TES observations presented here have a nadir footprint of approximately 5 km across track and 8.5 km along track, with a spacing of $\sim$1.6° along the orbit track. An overview of the TES data products and recent observations with TES nadir CO measurements are described in *Osterman et al.* [2006], *Luo et al.* [2007a, 2007b], and *Rinsland et al.* [2006]. The global TES CO profiles at approximately 600 mbar between 25 January and 5 February 2006 are shown in Figure 5b, with the same color scale as previously. The chemical equator can clearly been seen in the Western Pacific region, although the change in magnitude is not as great as in the in situ measurements, reflecting the reduction in resolution of such features as a result of necessary averaging over an 11-day time period to obtain sufficient satellite spatial coverage, as well as averaging over the vertical column (approximately 5 km) and the higher tangent altitude of TES observations (mid-troposphere).

[28] To qualitatively examine transport to the UT, a plot of CO data (weekly gridded: January 29 to February 4 2006) obtained from the Microwave Limb Sounder (MLS) data at 215 hPa is shown in Figure 5c (Figure produced by Jonathon H. Jiang, Jet Propulsion Laboratory). MLS Version 2.2 data has been shown to be high by approximately a factor of two but the morphology has been shown to be consistent [*Livesey et al.*, 2008]; single profile precision is estimated to be 20 ppbv. Therefore the values have to be scaled down by a factor of two but the relative spatial enhancement over Indonesia is expected to be more robust. The thick black lines surround areas of deep convection and this satellite data implies the occurrence of elevated levels of CO within the upper troposphere. TES profiles for the same period at 215 hPa were plotted and also indicate enhanced CO over the TWP with maximum mixing ratios which are similar to MLS values divided by 2. This data is not presented here since there is currently less information available on the validity of this data [*Lopez et al.*, 2008] compared to the known bias of MLS. *Matsueda et al.* [1998] used canister sampling onboard commercial airliners between Japan and Australia in the period 1993–1996 to study pollutant concentrations and found elevated levels of CO in the upper troposphere (8.5–13 km) during October-November (up to 130 ppbv) over the Western Pacific. This was attributed to vertical transport, associated with deep convection of CO from biomass burning in SE Asia and N Australia. The results presented indicate that air being uplifted in the tropical warm pool region during the measurement period (Jan/Feb) was characterized by a combination of the generally more polluted Northern Hemispheric background chemical signature and extensive biomass burning plumes. Thus, deep convection in the Western Pacific region would appear an important mechanism for injecting large quantities of highly polluted air to the upper troposphere. Air transported by deep convection to the upper troposphere will have distinctive properties, compared with air transported by large-scale ascent. Uplifted VOCs of ground-level origin have longer chemical lifetimes in the TTL and, in the presence of nitrogen oxides, can provide a photochemical source of ozone in the upper troposphere.

7. Conclusions

[29] This case study provides evidence of a sharp gradient in boundary layer composition to the south of the main region of convection in the Tropical Warm Pool during the Austral monsoon, which was not coincident with the Intertropical Convergence Zone or monsoon trough. The position of this chemical equator in clear sky conditions allowed its chemical characteristics to be determined while crossing the boundary, rather than on either side as in previous studies. The boundary was found to be about 50 km wide, with a profound change from clean Southern Hemisphere to polluted Northern Hemisphere air. Both the scale and the vertical structure of the transition were well simulated by a global transport model without convection or mixing, showing that it resulted from advection and confluence rather than mixing. The combination of in situ measurements and satellite observations indicate that polluted boundary-layer air over the TWP is being entrained by local deep convection and transported rapidly to the upper troposphere. Given the importance of this region for the composition of the TTL, and therefore the global stratosphere, the future evolution of pollution in this area of rapid economic development could have extensive global influence. Further work is required to investigate under which meteorological conditions the CE is decoupled from the ITCZ.

[30] **Acknowledgments.** The authors wish to acknowledge everyone involved in the ACTIVE project, in particular the pilots and staff of the Airborne Research and Survey Facility. We thank NERC for funding the ACTIVE project. Thanks also go the Australian Bureau of Meteorology and in particular Peter May, for help during the campaign and for access to meteorological data. MLS data was provided by Jonathon Jiang at the Jet Propulsion Laboratory (JPL), California. Thanks also go to the TES science team at JPL. Fire count data was obtained from the World Fire Atlas project, the Data User Element of the European Space Agency, and plotted by Manasvi Panchal. We also thank the RAAF base, Darwin, for hosting the aircraft and campaign base, and for their logistical support.

References

Agarwal, J. K., and G. J. Sem (1980), Continuous-flow, single-particle-counting condensation nucleus counter, *J. Aerosol Sci.*, *11*, 343–352.

Allan, J. D., et al. (2003), Quantitative sampling using an Aerodyne aerosol mass spectrometer: 2. Measurements of fine particulate chemical composition in two UK cities, *J. Geophys. Res.*, *108*(D3), 4091, doi:10.1029/2002JD002359.

Allen, G., et al. (2008), Aerosol and trace-gas measurements in the Darwin area during the wet season, *J. Geophys. Res.*, *113*, D06306, doi:10.1029/2007JD008706.

Arino, O., S. Plummer, and D. Defrenne (2005), Fire disturbance: The ten years time series of the ATSR World Fire Atlas, paper presented at MERIS (A)ATSR Workshop 2005 (ESA SP-597), ESRIN, Frascati, Italy, 26–30 September 2005.

Baumgardner, D., W. Strapp, and J. E. Dye (1985), Evaluation of the forward Scattering Spectrometer Probe-Part II: Corrections for coincidence and dead-time losses, *J. Atmos. Oceanic Technol.*, *2*, 626–632.

Beer, R., T. A. Glavich, and D. M. Rider (2001), Tropospheric emission spectrometer for the Earth observing system's Aura satellite, *Appl. Opt.*, *40*, 2356–2367.

Bowman, K. P., and P. J. Cohen (1997), Interhemispheric exchange by seasonal modulation of the Hadley circulation, *J. Atmos. Sci.*, *54*, 2045–2059.

Draxler, R. R., and G. D. Rolph (2003), HYSPLIT (HYbrid Single-Particle Lagrangian Integrated Trajectory) model access via NOAA ARL READY Website. NOAA Air Resources Laboratory, Silver Spring, MD. (Available at http://www.arl.noaa.gov/ready/hysplit4.html)

Gregory, G. L., et al. (1999), Chemical characteristics of Pacific tropospheric air in the region of the Intertropical Convergence Zone and South Pacific Convergence Zone, *J. Geophys. Res.*, *104*, 5677–5696.

Jayne, J. T., D. C. Leard, X. F. Zhang, P. Davidovits, K. A. Smith, C. E. Kolb, and D. R. Worsnop (2000), Development of an aerosol mass spectrometer for size and composition analysis of submicron particles, *Aeros. Sci. Tech.*, *33*, 49–70.

Jensen, P., and A. D. Del Genio (2003), Radiative and microphysical characteristics of deep convective systems in the tropical western Pacific, *J. Appl. Meteorol.*, *42*, 1234–1254.

Jimenez, J. L., et al. (2003), Ambient aerosol sampling using the Aerodyne Aerosol Mass Spectrometer, *J. Geophys. Res.*, *108*(D7), 8425, doi:10.1029/2001JD001213.

Kondo, Y., et al. (2004), Impacts of biomass burning in Southeast Asia on ozone and reactive nitrogen over the western Pacific in spring, *J. Geophys. Res.*, *109*, D15S12, doi:10.1029/2003JD004203.

Law, K. S., P. H. Plantevin, V. Thouret, A. Marenco, W. A. H. Asman, M. Lawrence, P. J. Crutzen, J. F. Muller, D. A. Hauglustaine, and M. Kanakidou (2000), Comparison between global chemistry transport model results and Measurement of Ozone and Water Vapor by Airbus In-Service Aircraft (MOZAIC) data, *J. Geophys. Res.*, *105*, 1503–1525.

Livesey, N. J., et al. (2008), Validation of Aura Microwave Limb Sounder O-3 and CO observations in the upper troposphere and lower stratosphere, *J. Geophys. Res.*, *113*, D15S02, doi:10.1029/2007JD008805.

Lopez, J. P., M. Luo, L. E. Christensen, M. Loewenstein, H. J. Jost, C. R. Webster, and G. B. Osterman (2008), TES carbon Monoxide Validation during two AVE Campaigns using Argus and ALIAS instruments on NSAS's WB-57F, *J. Geophys. Res.*, *112*, D16547, doi:10.1029/2007JD008811.

Luo, M., et al. (2007a), Comparison of carbon monoxide measurements by TES and MOPITT the influence of a priori data and instrument characteristics on nadir atmospheric species retrievals, *J. Geophys. Res.*, *112*, D09303, doi:10.1029/2006JD007663.

Luo, M., et al. (2007b), TES Carbon Monoxide validation with DACOM aircraft measurements during INTEX-B period, *J. Geophys. Res.*, *112*, D24S48, doi:10.1029/2007JD008803.

Matsueda, H., H. Y. Inoue, Y. Sawa, Y. Tsutsumi, and M. Ishii (1998), Carbon monoxide in the upper troposphere over the western Pacific between 1993 and 1996, *J. Geophys. Res.*, *103*, 19,093–19,110.

May, P. T., J. H. Mather, G. Vaughan, C. Jakob, G. M. McFarquhar, K. N. Bower, and G. G. Mace (2008), The Tropical Warm Pool International Cloud Experiment (TWPICE), *Bull. Am. Meteorol. Soc.*, *89*, 629–645.

Mitra, A. P. (2004), Indian Ocean Experiment [INDOEX]: An overview, *Indian J. Mar. Sci.*, *33*, 30–39.

O'Connor, F. M., K. S. Law, J. A. Pyle, H. Barjat, N. Brough, K. Dewey, T. Green, J. Kent, and G. Phillips (2004), Tropospheric Ozone Budget: Regional and Global Calculations, *Atmos. Chem. Phys. Disc.*, *4*, 991–1036.

Osterman, G., et al. (2006), Tropospheric Emission Spectrometer TES L2 Data User's Guide, 1 June 2006, Jet Propulsion Laboratory, California Institute of Technology, Pasedena, CA.

Reid, G. C., and K. S. Gage (1996), The tropical tropopause over the western Pacific: Wave driving, convection, and the annual cycle, *J. Geophys. Res.*, *101*, 21,233–21,241.

Rinsland, C. P., et al. (2006), Nadir measurements of Carbon Monoxide (CO) distributions by the Tropospheric Emission Spectrometer instrument onboard the Aura spacecraft: Overview of analysis approach and examples of initial results, *Geophys. Res. Lett.*, *33*, L22806, doi:10.1029/2006GL027000.

Savage, N. H., K. S. Law, J. A. Pyle, A. Richter, H. Nuss, and J. P. Burrows (2004), Using GOME NO2 satellite data to examine regional differences in TOMCAT model performance, *Atmos. Chem. Phys.*, *4*, 1895–1912.

Stehr, J. W., W. P. Ball, R. R. Dickerson, B. G. Doddridge, C. A. Piety, and J. E. Johnson (2002), Latitudinal gradients in O-3 and CO during INDOEX 1999, *J. Geophys. Res.*, *107*(D19), 8016, doi:10.1029/2001JD000446.

Thompson, A. M. (1992), The Oxidizing Capacity of the Earths Atmosphere-Probable Past and Future Changes, *Science*, *256*, 1157–1165.

Vaughan, G., C. Schiller, A. R. MacKenzie, K. N. Bower, T. Peter, H. Schlager, N. R. P. Harris, and P. T. May (2008), Studies in a natural laboratory: High-altitude aircraft measurements around deep tropical convection, *Bull. Am. Meteorol. Soc.*, *89*, 647–667.

Waliser, D. E., and C. Gautier (1993), A Satellite-Derived Climatology of the Itcz, *J. Clim.*, *6*, 2162–2174.

Williams, J., H. Fischer, S. Wong, P. J. Crutzen, M. P. Scheele, and J. Lelieveld (2002), Near equatorial CO and O-3 profiles over the Indian Ocean during the winter monsoon: High O-3 levels in the middle troposphere and interhemispheric exchange, *J. Geophys. Res.*, *107*(D19), 8007, doi:10.1029/2001JD001126.

G. Allen, K. N. Bower, J. Crosier, M. J. Flynn, and G. Vaughan, Centre for Atmospheric Science, University of Manchester, Simon Building, Oxforrd Road, Manchester, M13 9PL, UK.

G. D. Carver and N. R. P. Harris, Department of Chemistry, University of Cambridge, Lensfield Road, Cambridge, CB2 1EW, UK.

J. F. Hamilton, J. D. Lee, A. C. Lewis, J. E. Saxton, and N. M. Watson, Department of Chemistry, University of York, Heslington, York YO10 5DD, UK. (jfh2@york.ac.uk)

R. J. Parker and J. J. Remedios, Earth Observation Science, Space Research Centre, Department of Physics and Astronomy, University of Leicester, University Road, Leicester LE1 7RH, UK.

N. A. D. Richards, Institute for Atmospheric Science, School of Earth and Environment, University of Leeds, Woodhouse Lane, Leeds LS2 9JT, UK.